Singh Deepak (Orcid ID: 0000-0002-7247-7663)
Flanner Mark, Gregory (Orcid ID: 0000-0003-4012-174X)
Millour Ehouarn (Orcid ID: 0000-0003-4808-9203)

Improvement of Mars surface snow albedo modeling in LMD Mars GCM with SNICAR

D. Singh[1, 2], M.G. Flanner[2], E. Millour[3]

[1]Physical Research Laboratory, Ahmedabad, India

[2]Climate and Space Sciences and Engineering, University of Michigan, Ann Arbor, Michigan, USA

[3]Laboratoire de Météorologie Dynamique (LMD/IPSL), Sorbonne Universités, UPMC Univ Paris 06, PSL Research University, Ecole Normale Supérieure, Université Paris-Saclay, Ecole Polytechnique, CNRS, Paris, France

Corresponding author: Deepak Singh (sdeepak@umich.edu)

Key Points:

- We integrate the extended SNICAR snow model with LMD Mars GCM
- Updated model prognostically determines H_2O and CO_2 snow albedos interactively in the model
- Dust causes a substantial change in pure cryosphere albedo, and the global shortwave energy budget

This is the author manuscript accepted for publication and has undergone full peer review but has not been through the copyediting, typesetting, pagination and proofreading process, which may lead to differences between this version and the Version of Record. Please cite this article as doi: 10.1002/2017JE005368

Abstract

The current version of Laboratoire de Météorologie Dynamique (LMD) Mars GCM (original-MGCM) uses annually repeating (prescribed) CO_2 snow albedo values based on the Thermal Emission Spectrometer observations. We integrate the Snow, Ice, and Aerosol Radiation (SNICAR) model with MGCM (SNICAR-MGCM) to prognostically determine H_2O and CO_2 snow albedos interactively in the model. Using the new diagnostic capabilities of this model, we find that cryospheric surfaces (with dust) increase the global surface albedo of Mars by 0.022. Over snow-covered regions, SNICAR-MGCM simulates mean albedo that is higher by about 0.034 than prescribed values in original-MGCM. Globally, shortwave flux into the surface decreases by 1.26 W/m^2, and net CO_2 snow deposition increases by about 4% with SNICAR-MGCM over one Martian annual cycle as compared to original-MGCM simulations. SNICAR integration reduces the mean global surface temperature, and the surface pressure of Mars by about 0.87% and 2.5% respectively. Changes in albedo also show a similar distribution to dust deposition over the globe. The SNICAR-MGCM model generates albedos with higher sensitivity to surface dust content as compared to original-MGCM. For snow-covered regions, we improve the correlation between albedo and optical depth of dust from -0.91 to -0.97 with SNICAR-MGCM as compared to the original-MGCM. Dust substantially darkens Mars' cryosphere, thereby reducing its impact on the global shortwave energy budget by more than half, relative to the impact of pure snow.

1 Introduction

Surface albedo plays an important role in any planet's energy budget and driving its climate system. Water-vapor, cloud, and albedo feedbacks are the three most powerful positive feedback mechanisms operating within the current climate system on Earth [e.g., *Bony et al.,* 2006; *Winton,* 2006; *Randall et al.,* 2007; *Soden et al.,* 2008; *Shell et al.,* 2008; *Flato et al.,* 2013; *Singh et al.,* 2015]. Due to the small amounts of water-vapor on Mars (as compared to Earth) [e.g., *Jakosky and Farmer,* 1982; *Smith,* 2002; *Maltagliati et al.,* 2011], cloud (consisting

of condensed water or carbon dioxide) and albedo feedbacks are the primary feedback mechanisms of climate on Mars. Dust is a critical component of Martian climate [e.g., *Haberle et al.,* 1982; *Hourdin et al.,* 1995; *Clancy et al.,* 2000; *Newman et al.,* 2002a, 2002b; *Madeleine et al.,* 2011], and it can significantly amplify or weaken the other feedback mechanisms.

Dust is tightly coupled with the other components of the climate system. Global dust events can cause changes in meteorological phenomena (i.e., dust storms, dust devils, clouds, recession of the polar caps, and surface temperatures) that can persist for periods ranging from a few weeks to more than one Mars year [*Cantor,* 2007; *Montabone et al.,* 2015; *Wang and Richardson,* 2015; *Guzewich et al.,* 2017]. The dust and CO_2 cycles have long been known to greatly affect the present-day climate of Mars. Although dust cycles are highly variable on Mars, the CO_2 condensation cycle is highly repeatable on multi-annual timescales [*Hess et al.,* 1980; *Kieffer and Titus,* 2001; *Brown et al.,* 2010; *Brown et al.,* 2012]. Viking landers measurements (VL1 and VL2) show a highly variable dust cycle (including large dust storms) over the years [e.g., *Zurek and Martin,* 1993]. Snow albedo is strongly affected by the amount, types, and sizes of dust impurities present in the snow [e.g., *Wiscombe and Warren,* 1980; *Warren,* 1984; *Kieffer,* 1990; *Singh and Flanner,* 2016].

The current version of the Laboratoire de Météorologie Dynamique (LMD) Mars GCM (hereafter original-MGCM) uses annually repeating albedo values for CO_2 snow, derived from the Thermal Emission Spectrometer (TES) observations, and a constant albedo value for H_2O snow-covered surfaces. These observations also show significant seasonal variation of snow (both H_2O and CO_2) albedo [*Kieffer et al.,* 2000; *Kieffer and Titus,* 2001]. Small changes in albedo can have strong impacts on Martian climate dynamics, especially due to the very low surface pressure (<1% of Earth's atmosphere). Changes in albedo will alter the heating rate at the surface, therefore affecting the CO_2 snow sublimation rate, and hence the Mars CO_2 cycle [e.g., *Wood and Paige,* 1992; *Hourdin et al.,* 1995; *Brown et al.,* 2016]. Therefore, it is important to

prognostically determine snow (both H_2O and CO_2) albedos interactively in models of Mars' climate.

In this paper, we use the framework of *Singh and Flanner* [2016] to integrate the extended Snow, Ice, and Aerosol Radiation (SNICAR) model [*Flanner* et al., 2007; *Flanner* et al., 2009] with the original-MGCM to simulate the impact of H_2O and CO_2 snow albedo on the Martian energy budget. We then analyze subsequent changes in the Mars CO_2, temperature, and pressure cycles. We perform multiple analyses to determine the sensitivity of the Martian energy budget to cryospheric surfaces and dust presence in snow. We also compare our simulations with observed Mars surface pressure from VL1 measurements. Finally, we assess the correlation between atmospheric dust and snow albedo on Mars in simulations with and without prognostic snow albedo.

2 Methodology

We incorporate the extended SNICAR model into the original-MGCM to calculate real-time interactive surface broadband snow albedo. SNICAR is a two-stream multiple scattering radiative transfer model used to simulate the albedo, transmission, and vertical absorptivity of snow surfaces consisting of different mixtures and size distributions of H_2O snow, CO_2 snow, and light-absorbing impurities like dust [e.g., *Flanner et al.*, 2007; *Singh and Flanner*, 2016]. It has been applied extensively to represent terrestrial snow surfaces, and details of model adaptation and model evaluation for Martian cryospheric surfaces are described by *Singh and Flanner* [2016]. The extended version of SNICAR utilizes 480 bands spanning 0.2-5.0 μm at 10 nm spectral resolution. We divide the broadband (0.2-5.0 μm) into two sub-regions (0.2-0.5 μm and 0.5-5.0 μm) which are used for atmospheric radiative transfer calculations in the original-MGCM. These band-averaged values are weighted with solar spectral irradiance measurements from *Labs and Neckel* [1968]. We use the optical properties [*Singh and Flanner*, 2016] of Martian dust [*Wolff* et al., 2006; *Wolff* et al., 2009; *Wolff* et al., 2010] determined using Mie

Theory with an assumed gamma size distribution [*Hansen and Travis*, 1974] with r_{eff} = 1.5μm and effective variance (υ_{eff}) = 0.3 [*Wolff* et al., 2006].

2.1 Original-MGCM scheme

The original-MGCM described in *Pottier et al*. [2017] and includes schemes to account for the CO_2 [*Forget et al.* 1998; 1999], water [*Navarro et al.*, 2014], and dust [*Madeleine et al.*, 2011] cycles. As demonstrated in *Haberle et al.*, [2008], the presence of sub-surface polar water ice tables act as heat reservoirs and significantly impact the CO_2 cycle, along with CO_2 snow albedo and emissivity values [*Wood and Paige*, 1992]. Thus to correctly tune the original-MGCM CO_2 cycle (i.e. to obtain surface pressures at VL1 site which match the observations), following *Hourdin et al.*, [1995], a minimizing technique to optimize north and south sub-surface water ice table depths and surface CO2 snow albedo is initially used. In addition, to improve the realism of the modeled CO_2 cycle, when CO_2 snow is present at the surface, its albedo is set to the broadband albedo measured by the TES solar channel times a tuning coefficient to account for the effect of airborne dust on measurements and the non-Lambertian behavior of the snow (this coefficient is also optimized to obtain a better fit when comparing to the VL1 annual pressure cycle).

Instead of using a prescribed surface albedo from TES observations, SNICAR coupled with the original-MGCM (SNICAR-MGCM) calculates the surface albedo (of both H_2O and CO_2 deposits) interactively using surface dust deposition flux (already present in the model) as an input. As pure snow albedos are much higher [*Singh and Flanner*, 2016] than the TES observed albedos, a first step in this process was to determine a base amount of dust to constrain simulated albedos within realistic limits. First the original model was run for a long period with dust accumulation in snow occurring throughout the run. We calculate accumulated dust and SNICAR albedos as diagnostic variables for this purpose. The accumulated dust amount at the time-step (~550 sols) for which minimum difference between annual global averages of TES observed albedo and modeled albedo is achieved is used as a "baseline dust" for model

initialization. This albedo difference was minimized only for snow-covered regions. The "baseline dust" varies spatially, and has the same surface grid-resolution as the original-MGCM.

2.2 Dust Scheme

The next step in the process was to simulate realistic amounts of dust in snow for long duration model runs. The original-MGCM uses a prescribed airborne dust climatology [*Montabone et al.*, 2015] specific to each Martian year. This dust scheme is semi-interactive, which uses a virtual tracer to keep track of the dust content in the atmosphere and that the scheme implies adding a flux of that virtual tracer from the surface (which is vertically transported by the GCM's turbulence scheme, sediments, etc.; that tracer is also advected by the dynamics) at all locations and times. The columnar value of this virtual tracer is then rescaled to match the column optical depth to be prescribed using the dust scenario. In that sense, the total (column) amount of dust is prescribed, but not the shape of the vertical profile. Once the rescaling done, one has access to a dust vertical profile from which one may derive an evaluation of vertical dust gradient, dust fallout etc. We do not enforce (or track) any conservation of dust (again because we prescribe the columnar amount of dust).

We used an exponential decay mechanism to achieve stable dust amounts in snow. Our dust scheme is an implicit dust removal function that we incorporated to prevent dust burdens in perennial ice from continuously increasing. The chief physical process on Mars that is likely responsible for dust removal from permanent ice is exposure of dust deposits from sublimation, followed by wind scouring and remobilization. Adequately resolving these processes, however, would require a multi-layer fine resolution snow model that keeps track of very thin dust deposit layers. Since we cannot explicitly resolve re-exposure of dust and wind scouring with the bulk (single layer) snow model in the original-MGCM, we incorporate it as an implicit e-folding decay scheme. In rare circumstances, snow and ice melt may also carry dust particles down through the ice column into the underlying soil, but vertical redistribution of dust particles also cannot be resolved without a multi-layer model, hence this process is also represented implicitly

in our decay scheme. Finally, we note that when seasonal ice is completely eliminated from the surface, dust concentrations in snow are reset to zero in advance of any subsequent ice deposition, thus effectively removing any dust that had been in the snow. When the snow melts or sublimates completely, the dust is effectively transferred back to the soil. For a given time '*t*', net dust burden in snow (kg/m^2) in snow $d(t)$ at the surface is given by:

$$d(t) = \left[d(t-1) + d_0\right] e^{-t_0/\tau} \quad (1)$$

where 'd_0' is the dust deposition (at surface) occurring during the time step in the original-MGCM, 't_0' is the physical time-step (1/96 sol; 1 sol = 88775 seconds) of the model run, and 'τ' is the decay constant. For t = 0, we use baseline dust to represent $d(t-1)$. To calculate the value of 'τ', we first run the model for one Martian Year (MY) without any decay mechanism. Next, we replace $d(t)$ with the average baseline dust determined earlier, $\left[\left(d(t-1) + d_0\right)\right]$ with average model accumulated dust at the end of run, and 't_0' with the total run-time (in seconds) of the model. We found the optimal value of 'τ' to be equal to 1.36×10^8 seconds (~1528 sols) using above mentioned technique.

Here, the relaxation timescale for dust burdens in snow is spatially uniform. As shown later, the optimal timescale that we found produces stable global burdens of dust in snow, but we acknowledge that removal timescales must vary spatially. Exponential decay scheme is easy, and robust to implement without hampering the actual dust content calculations much. Understanding and implementation of a more sophisticated decay mechanism would require a separate study, and a different approach. More sophisticated and vertically-resolved snow models will enable future removal schemes to be coupled more closely to model physics.

2.3 Coupling with SNICAR

Finally, we couple the extended version of SNICAR [*Singh and Flanner*, 2016] with the original-MGCM to provide more physically realistic albedo simulations for snow covered

surfaces, and higher spectral resolution (different albedo for each wavelength band in original-MGCM). We also determine the impact of cryospheric surfaces and dust in snow on the shortwave energy flux of Mars. In this study, all grid-boxes with at least 0.01 kg/m^2 surface snow are considered part of the "snow-covered" region. We assume zero change in all physical quantities at non-snow covered regions for all scenarios in this study. Therefore changes over non-snow covered regions are not plotted in any maps, except the dust deposition at surface. All global average parameters are area-weighted means for that particular quantity. Snow-covered averages are area-weighted means for snow-covered regions only. We determine the Pearson correlation coefficient to measure the linear correlation between two variables. All the changes reported in this paper are with respect to the original-MGCM, unless stated otherwise.

3 Results and Discussion

We run the original-MGCM for various Martian Years (MY24 – MY31) [*Clancy et al.,* 2000] using separate dust climatologies [*Montabone et al.,* 2015] specific to each year. Figure 1 shows the global annual mean surface albedos for various scenarios on Mars. Snow-free albedo is bare ground albedo (prescribed in the model) without the presence of any snow. MGCM albedo is that simulated using the original-MGCM (without SNICAR), Dust-free albedo is pure snow albedo as simulated with the integrated version of SNICAR but assuming no dust in snow, and finally SNICAR albedo is the albedo computed after the integration of SNICAR into the MGCM (SNICAR-MGCM) and including the effects of dust in snow. Due to higher sensitivity to dust, SNICAR albedos are slightly lower than original-MGCM albedos for Martian Years with higher dust deposition (e.g. MY25), and higher for years with lower dust deposition (e.g. MY30). We observe a correlation of 0.861 between annual mean values of SNICAR-MGCM and original-MGCM surface albedo (area weighted average over snow-covered area). Dust-free and snow-free albedos are derived from diagnostic dust-free and snow-free albedo calculations respectively within the original-MGCM. These diagnostic calculations are computed within the same simulation. However, the diagnostic calculations do not affect the simulated climate state.

The global annual mean values differ little between the original-MGCM and SNICAR-MGCM scenarios (Table 1), indicating physical stability of the model with SNICAR integration. Table 1 also presents mean albedo values calculated over snow-covered surface only. Dust-free albedos are much higher than the SNICAR-MGCM albedos due to the presence of high amounts of light-absorbing dust within snow in the latter case. We also note that CO_2 snow is more susceptible to dust darkening as compared to H_2O snow, especially in the near-IR spectral region [*Singh and Flanner*, 2016]. Table 2 lists the changes caused in net surface shortwave flux between various scenarios discussed in the following sections.

Table 1: Eight Martian years (MY24-MY31) annual mean albedo for various scenarios on Mars. All means are area-weighted.

Scenario	**SNICAR**	**MGCM**	**Dust-free (with SNICAR)**	**Snow-free**
Mean Albedo (Global)	0.23	0.23	0.29	0.20
Mean Albedo (Snow-covered)	0.41	0.37	0.73	0.20

Table 2: Surface shortwave flux changes between various scenarios (Scenario 1 – Scenario 2) discussed in this paper.

Scenario 1	**Scenario 2**	**Global (W/m^2)**	**Snow-covered (W/m^2)**
SNICAR-MGCM	Original-MGCM	-1.26	-6.79
Snow mixed with dust	No cryosphere	-0.44	-2.25
Snow mixed with dust	Pure snow	0.25	3.33

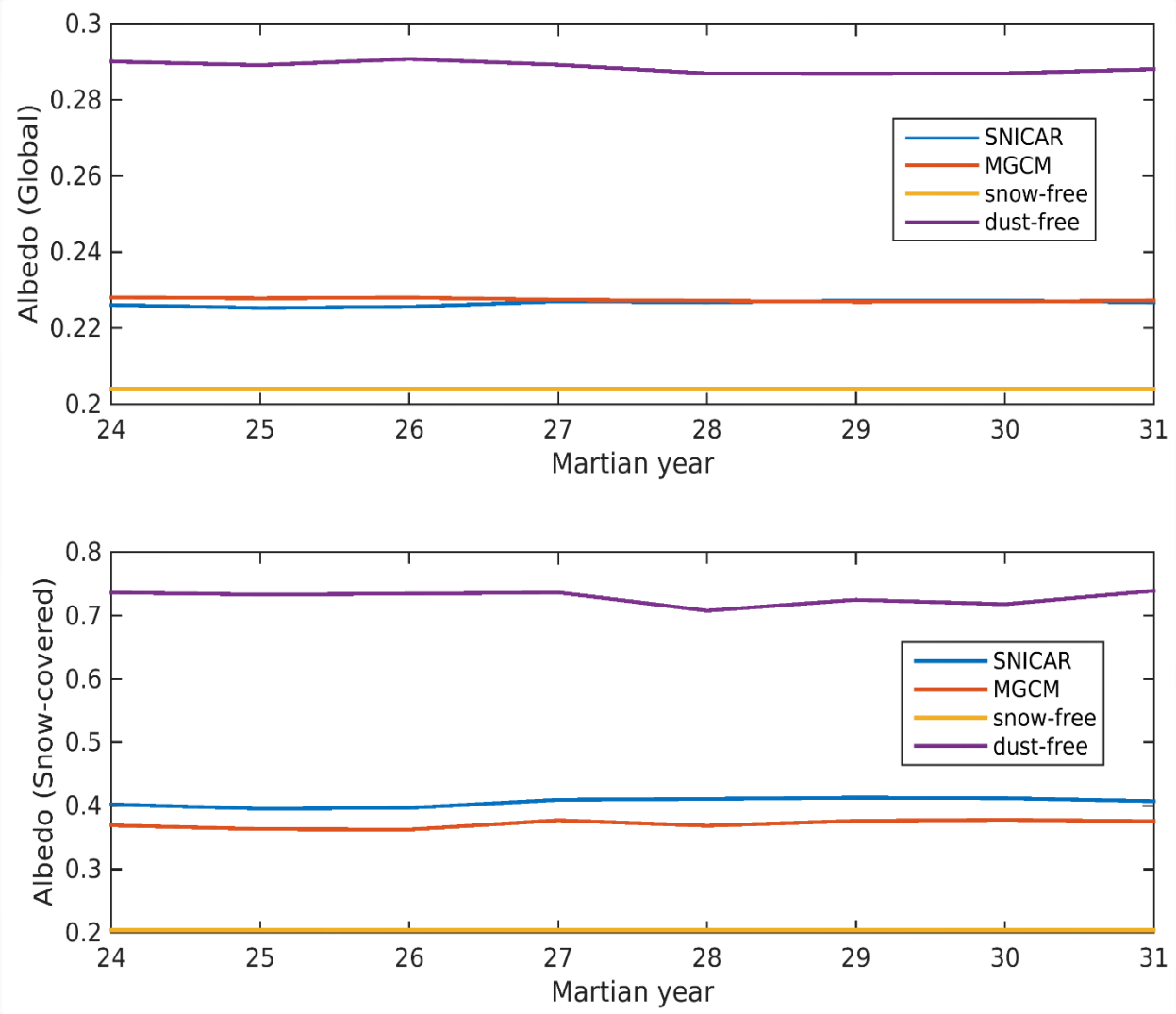

Figure 1: Annual global (top) and snow-covered (bottom) mean surface albedo of Mars calculated for various scenarios.

3.1 Comparison between SNICAR-MGCM and original-MGCM simulations

Figure 2a shows the global map of difference in annual mean albedo simulated using SNICAR-MGCM and original-MGCM (SNICAR minus MGCM albedo). In general, SNICAR-MGCM albedos are higher than original-MGCM albedos near the poles and are smaller near

mid-latitudes. Original-MGCM simulates much higher dust deposition near mid-latitudes as compared to the poles (Figure 2b), resulting in lower snow albedo simulated by SNICAR-MGCM. This effect was not present in the original-MGCM because the albedo was insensitive to dust variability on the surface. Albedo changes also follow a similar distribution as the surface dust deposition (positive with lower dust deposition and negative with higher dust deposition), especially in Northern Hemisphere. We observe a larger change in albedo in Southern Hemisphere due to higher abundance of CO_2 snow [e.g., *Kieffer et al.*, 2000], which is brighter than H_2O snow [*Singh and Flanner*, 2016]. These changes in albedo significantly impact the shortwave flux, especially at the surface (Figure 3).

We do not observe a direct correlation between change in the albedo and net shortwave flux because of high variation in the atmospheric dust content from one year to another on Mars. Due to global dust storms (e.g. MY25), the amount of dust in the atmosphere increases by almost a factor of two from the previous year. Atmospheric dust can significantly change the downwelling flux, therefore it acts as an important contributing factor for change in the net shortwave flux. After the SNICAR integration, we estimate global (snow-covered) annual mean change in albedo and net shortwave flux (at surface) of 0.001 (0.034) and -1.26 (-6.79) W/m^2, respectively, relative to the original-MGCM. Since the SNICAR-MGCM uses higher dust content in the snow as compared to the original-MGCM, the dust have a significant effect on the downwelling flux in snow-covered regions. Due to relatively higher dust deposition in mid-latitudes, the downwelling flux increase substantially. Generally, this causes SNICAR-MGCM obtained net shortwave flux to be lower than mean original-MGCM net shortwave flux.

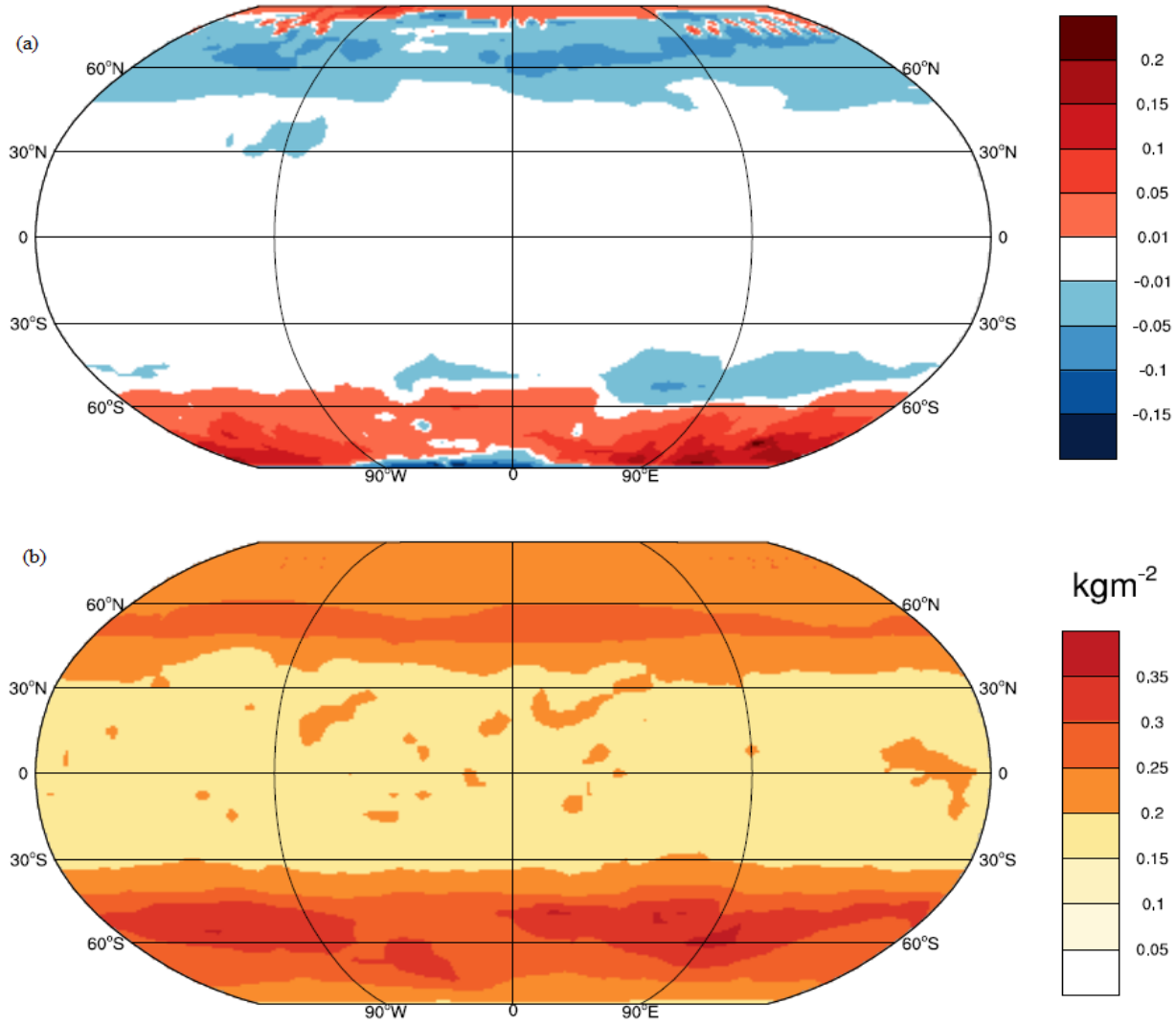

Figure 2: Eight Martian years (MY24-MY31) annual mean maps highlighting (a) mean albedo difference between SNICAR-MGCM and original-MGCM (mean SNICAR-MGCM albedo – mean original-MGCM albedo); (b) mean surface dust deposition.

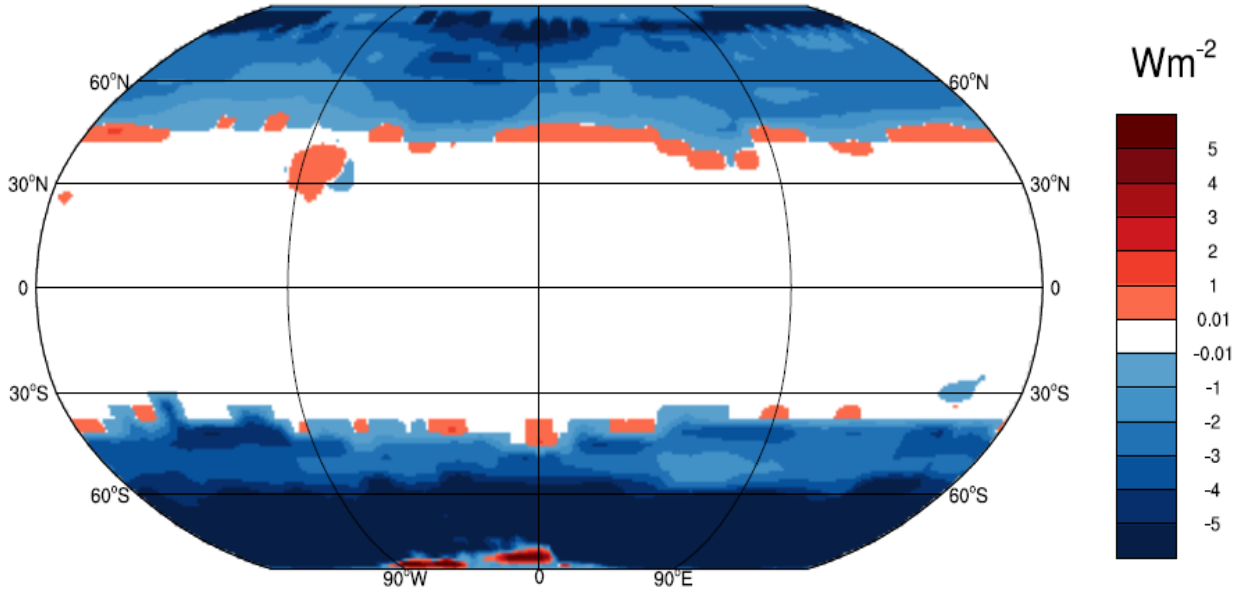

Figure 3: Global map of mean shortwave flux difference at the surface between SNICAR-MGCM and original-MGCM (mean SNICAR-MGCM flux – mean original-MGCM flux).

Due to albedo changes imparted by the SNICAR integration, we observe an average net increase (~ 4%) of CO_2 snow deposition on Mars surface over one annual cycle (Figure 5a) as compared to the original-MGCM simulations. On average all regions experience an increase in CO_2 snow deposition, except at (and nearby) the South Pole (Figure 4). SNICAR integration reduces the net mean global surface temperature (Figure 5b) of Mars by about 1.7 K (0.87%), with variation in temperature drop ranging from 1.5 K for high-dust years (e.g. MY25) to 2.0 K for low-dust years (e.g. MY30). This leads to the conclusion that the polar albedo increase and associated temperature drop caused by SNICAR integration are primarily responsible for higher CO_2 snow surface deposition. Due to higher CO_2 deposition, we also observe a net reduction of about 2.5% in the surface pressure (Figure 5c) annually.

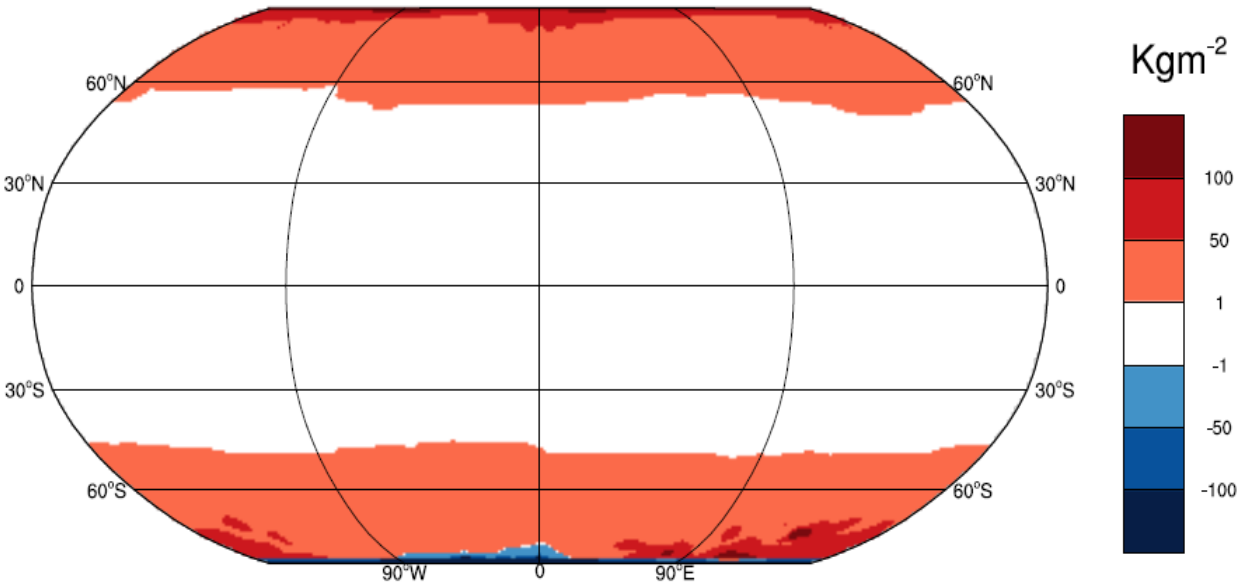

Figure 4: Global map of net annual mean CO_2 snow deposition difference between SNICAR-MGCM and original-MGCM (mean SNICAR-MGCM CO_2 snow deposition – mean original-MGCM CO_2 snow deposition).

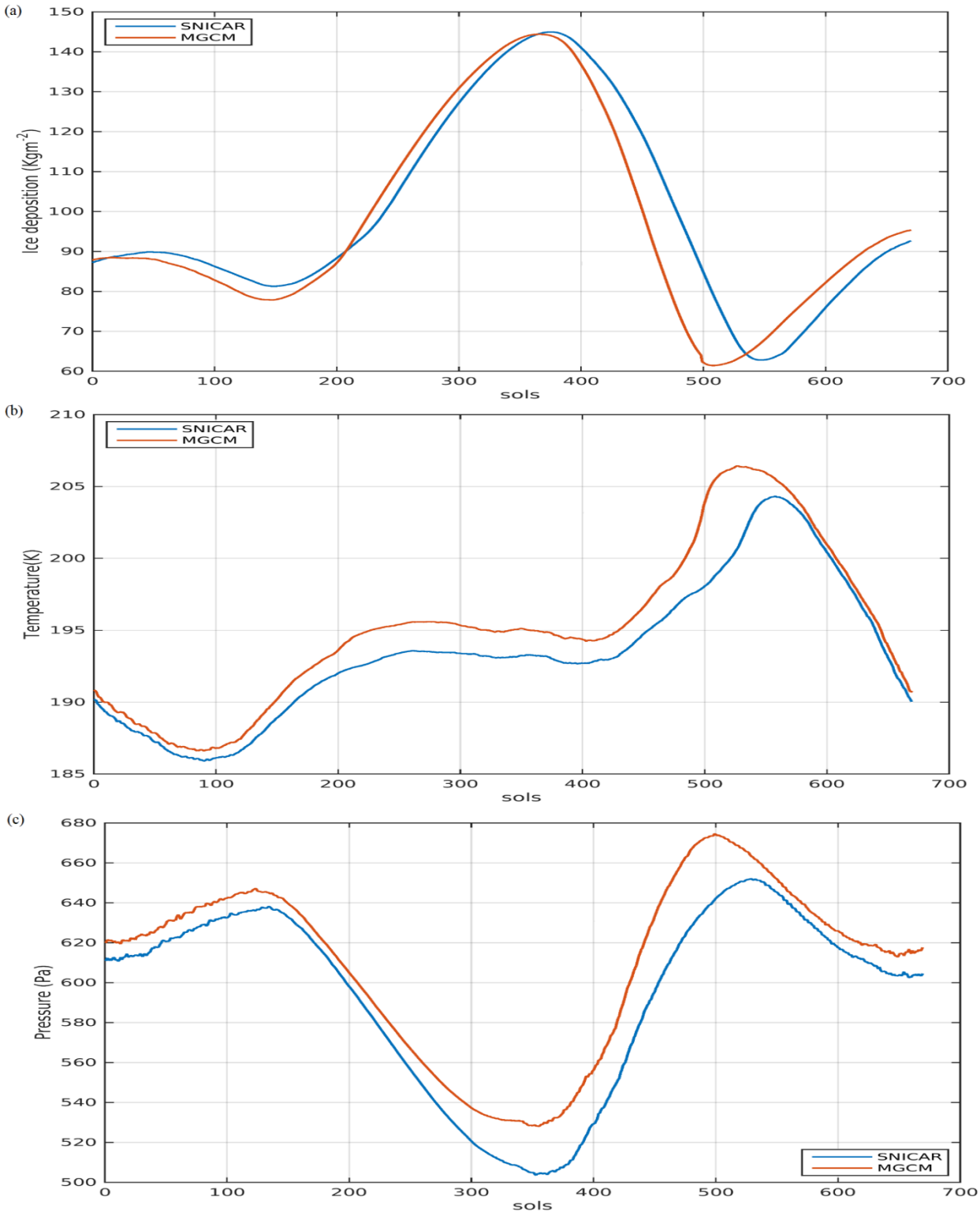

Figure 5: Annual variation (1 MY ≈ 669 sols) of global means for (a) net CO_2 snow deposition (top), (b) surface temperature (middle), and (c) surface pressure (bottom). Values are averaged over eight Martian years (MY24-MY31).

3.2 Comparison between snow-covered and snow-free scenarios

After integrating SNICAR into the original-MGCM, we estimate the impact of cryospheric cover on Martian albedo and shortwave energy flux via diagnostic calculations. Both snow-free and snow-covered simulations are performed using the dust scheme described in section 2.2. Snow-free calculations are separate diagnostic output calculated within the same simulation. However, being a diagnostic output, snow-free calculations do not alter the simulated climate state. We determine the net content of dust in snow using both original-MGCM predicted dust deposition flux and baseline dust along with the decay mechanism (Equation 1). Figure 6 shows the global difference map of bare ground albedos from snow-covered albedos. Some grid-points near the mid-latitudes show a slightly higher albedo for bare ground as compared to snow-covered albedo. In these regions snowfall frequency and amount are both lower as compared to polar regions. A high concentration of dust within a small amount of snow can decrease the surface albedo significantly, and bring it lower than the actual bare ground albedo. Also, the strong absorption features of CO_2 snow at various wavelengths disappear with high dust concentrations [*Singh and Flanner*, 2016]. Figure 7 shows the changes in shortwave energy flux at the surface between snow-covered and snow-free scenarios. On Mars, the cryosphere causes a global (snow-covered) annual mean change of 0.022 (0.202) and -0.44 (-2.25) W/m^2 in albedo and net surface shortwave flux respectively, compared to there being bare ground at these locations. The global annual-mean net surface shortwave flux on Mars is currently about 120 W/m^2.

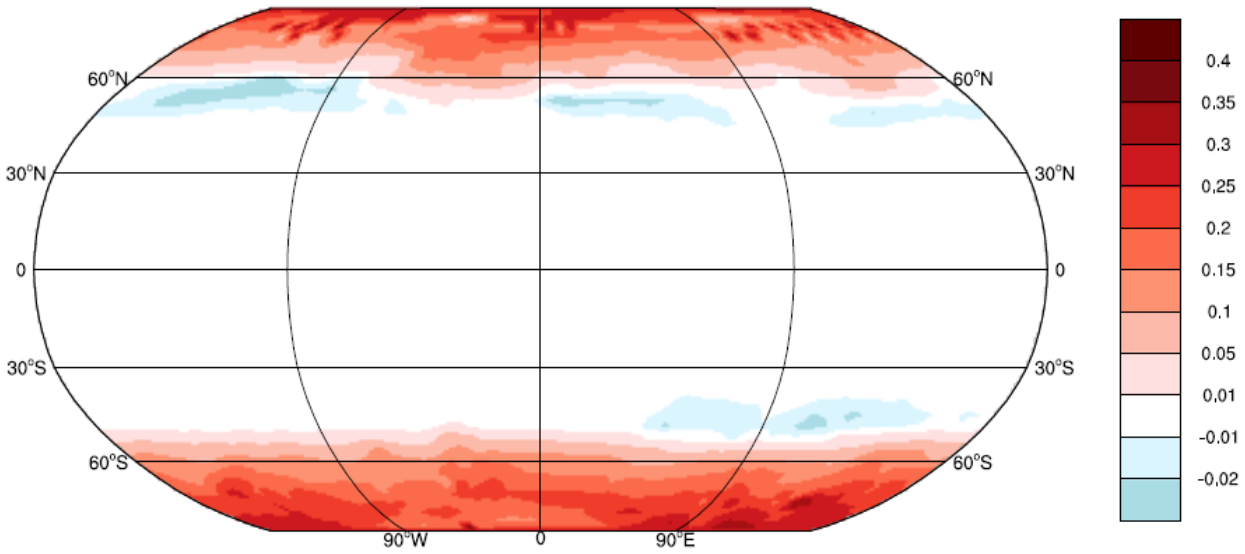

Figure 6: Global map of mean albedo difference between snow-covered and snow-free albedo

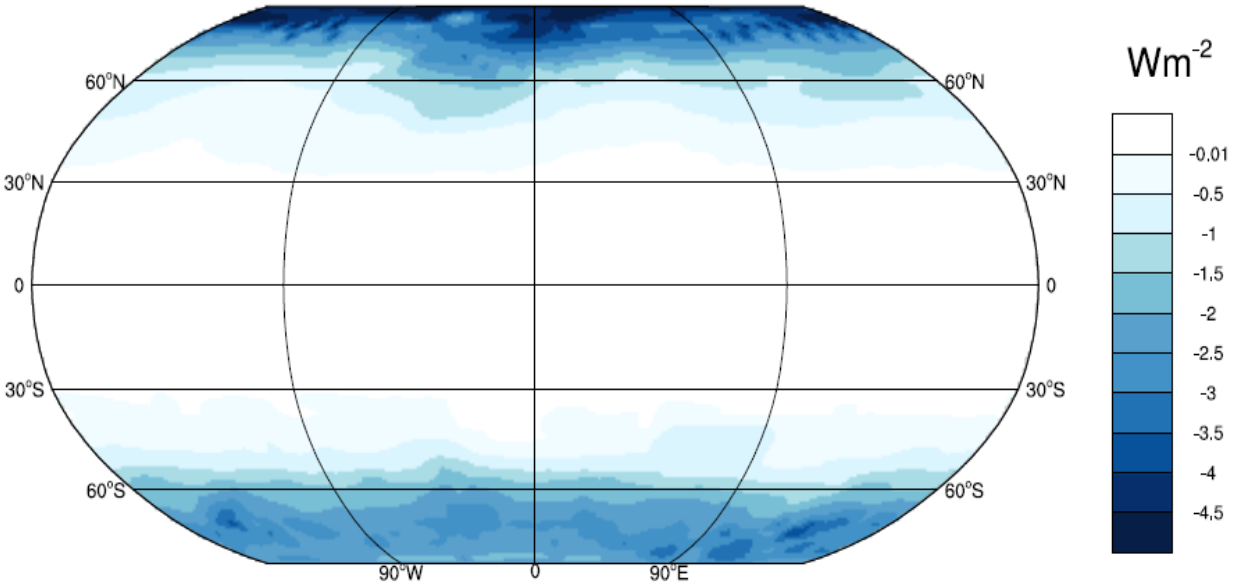

Figure 7: Global map of mean shortwave flux difference at the surface between snow-covered and snow-free scenarios using SNICAR-MGCM.

3.3 Impact of dust

Next we calculate the impact of dust darkening on Martian snow albedo and shortwave energy flux. As for the snow-free calculations, dust-free calculations are also diagnostic outputs, and they do not alter the simulated climate state. Net global (snow-covered) annual mean dust-free albedo is higher by about 0.06 (0.32) than the actual albedo calculated using the SNICAR-MGCM (Figure 8). Differences are negligible near the cap edge due to the scarcity of snow. Except for those edges, the albedo change is higher near mid-latitudes as compared to the poles. This happens due to the decrease in dust amount from mid-latitudes to poles (Figure 2b). Dust causes a global (snow-covered) annual mean change of 0.25 (3.33) W/m^2 in shortwave flux at the surface, compared to there being pure snow at the snow-covered locations (Figure 9). The absolute change in albedo caused by dust in snow (for snow-covered regions) relative to pure snow is larger than the albedo change caused by the dusty cryosphere relative to the bare ground. This illustrates the importance of dust in the Martian climate system.

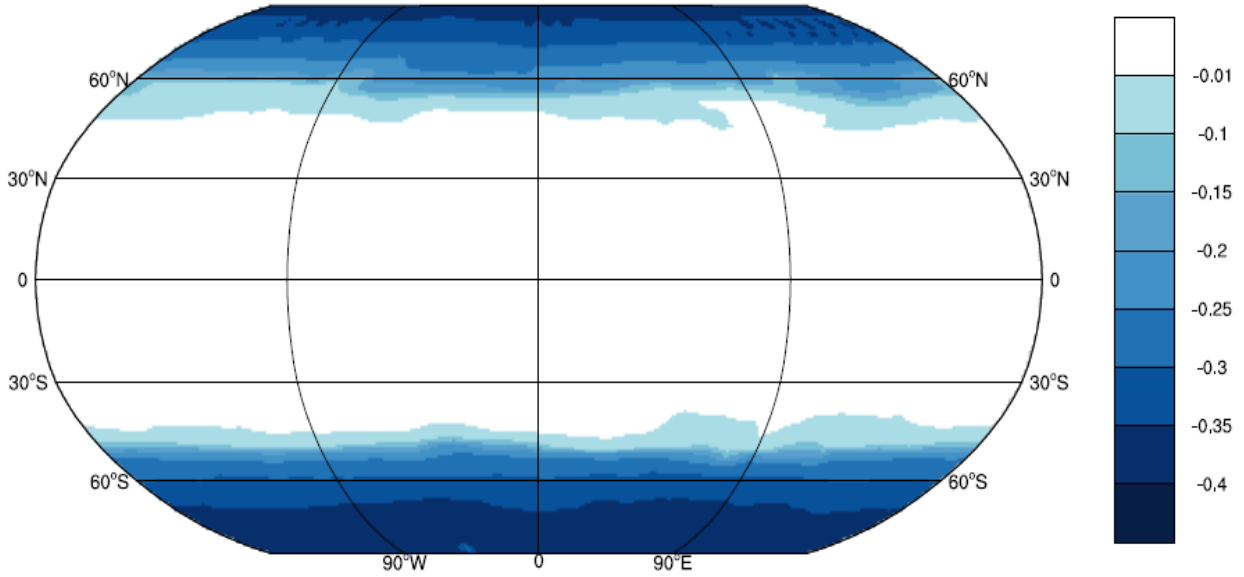

Figure 8: Global map of mean albedo difference between SNICAR-MGCM albedo and SNICAR-MGCM dust-free albedo.

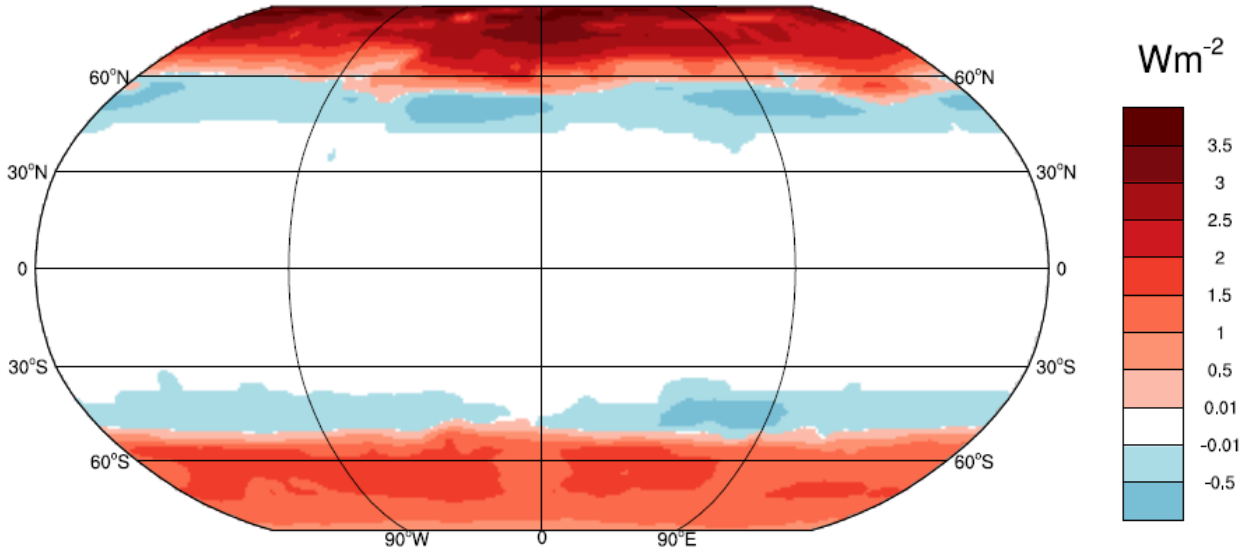

Figure 9: Global map of mean shortwave flux difference at the surface between SNICAR-MGCM albedo and dust-free scenarios using SNICAR-MGCM.

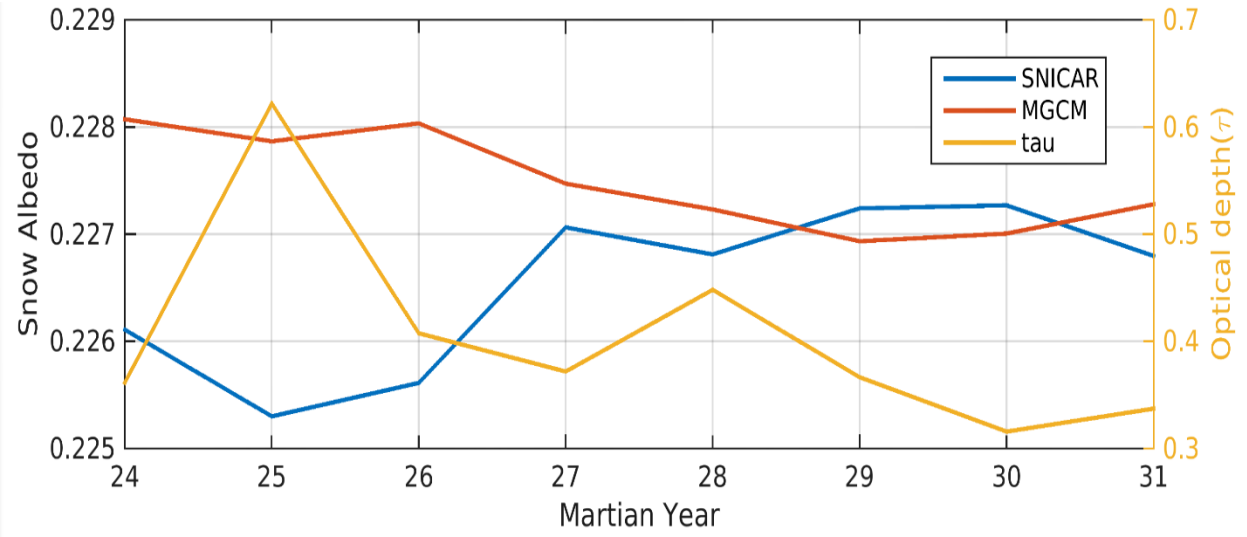

Figure 10: Global annual mean of snow albedos using SNICAR-MGCM and original-MGCM, and optical depth of dust for various Martian years.

We observe a higher sensitivity of surface albedo to atmospheric dust with SNICAR-MGCM, as shown in Figure 10. We initially observe that the original-MGCM albedos are not very sensitive to dust optical depth over the years. For snow-covered regions, we improved the correlation between albedo and dust optical depth from -0.91 to -0.97 with SNICAR-MGCM as compared to the original-MGCM. We use global annual values from eight Martian Years (Figure 9) to compute correlation coefficients. In general, net snow-albedo decreases with increasing dust content in the snow [e.g., *Singh and Flanner,* 2016]. Since the dust optical depth is directly correlated with dust deposition, an anti-correlation is expected between albedo and optical depth. Therefore more negative correlation coefficient indicates a better agreement between the two quantities. On a global scale, albedo and optical depth have a positive correlation of 0.41 in original-MGCM, indicating no relationship between the two quantities. This happens because the original-MGCM uses prescribed TES surface albedo irrespective of dust content. We observe a correlation of -0.72 between albedo and optical depth with SNICAR-MGCM on a global scale.

3.4 Comparison with observed data

Finally, we compare our simulated surface pressures (diurnal averages) with VL1 observed surface pressures (diurnal averages). The Viking lander (VL1) recorded surface pressure data for Mars at a particular location in Northern Hemisphere (22.5°N, 48°W) [e.g., *Hess et al.,* 1980; *Hourdin et al.,* 1993]. First, we extract the pressure data from the original-MGCM and the SNICAR-MGCM runs at VL1 location with a hydrostatic rescaling to the actual Viking Lander altitude to enable comparisons with the Viking Lander records. Next, we average this surface pressure data over eight Martian years (MY24-MY31). Lastly, we compare this rescaled and averaged surface pressure data with observed surface pressure data (VL1). The original-MGCM yields an average difference of about 6% in the surface pressure as compared to VL1 (Figure 11). Comparatively, the SNICAR-MGCM yields an average difference of about 8.4% in the surface pressure as compared to VL1 (Figure 11) observed surface pressure. The simulated surface pressure reduction with the SNICAR-MGCM is consistent with the global reduction of

2.5% in surface pressure discussed in section 3.1. This annual offset between model and observations in surface pressure is not fundamental. This can be easily minimized with changing global atmospheric mass in the model. This comparison illustrates the impact of introducing SNICAR with respect to the original-MGCM, and the resulting shift in CO_2 polar caps progression and regressions. For full evaluation of the SNICAR-MGCM scheme with respect to the observations, one should re-tune the CO_2 cycle (using the same procedure as used for the original-MGCM, described in section 2.1), which is beyond the scope of this paper.

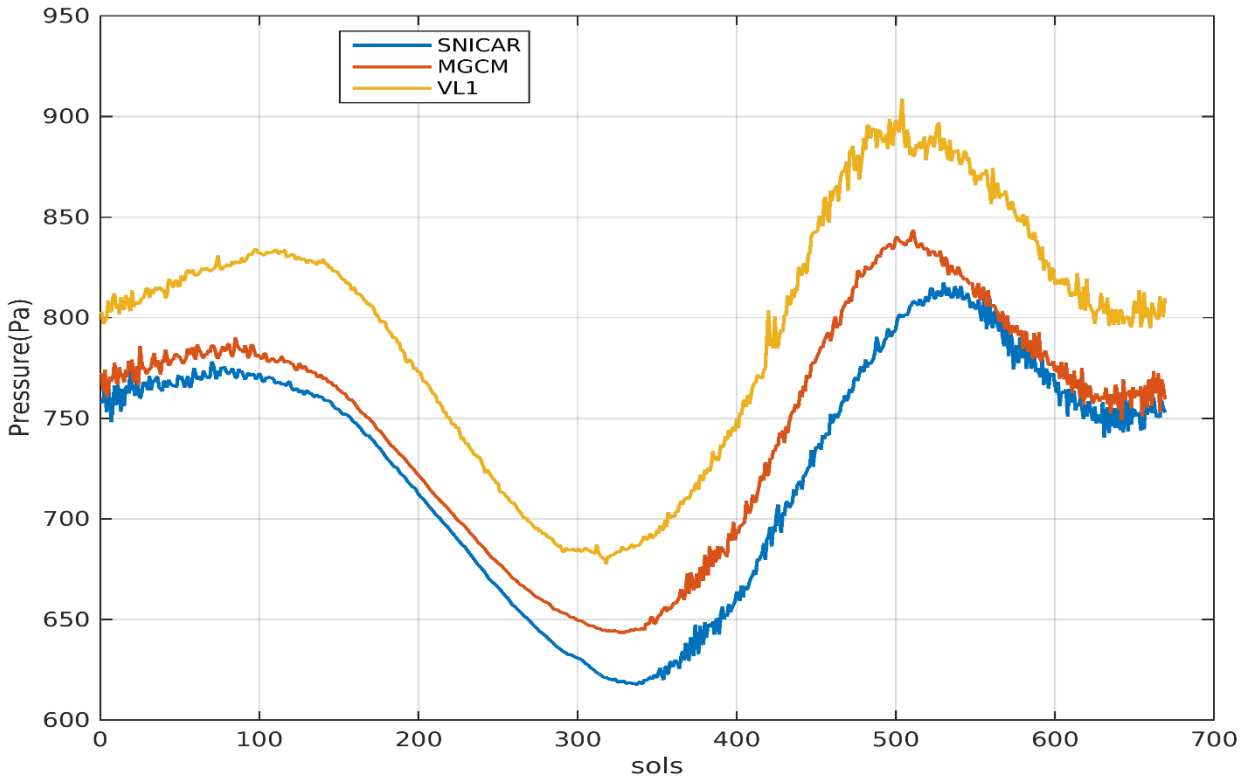

Figure 11: Comparison of annual variation of surface pressure at VL1 landing site along with the same (see text) obtained with the original MGCM and SNICAR-MGCM simulations.

4 Conclusions

We successfully integrate the extended version of SNICAR [*Singh and Flanner,* 2016] into the current version of the LMD Mars GCM to calculate real-time interactive snow albedo, dependent on dust deposition fluxes determined by the model. We use a baseline dust content to constrain the surface albedo within realistic boundaries for Mars. We also use an implicit exponential decay method to release dust on the surface over time.

On a global scale, there is no significant difference between SNICAR-MGCM and original-MGCM surface albedo. However, the SNICAR-MGCM model generates albedos with higher sensitivity to surface dust content as compared to the original-MGCM. In some cases SNICAR-MGCM albedo is smaller because of higher dust in that region. SNICAR integration also alters the planet's CO_2 cycle. On a global scale, net CO_2 snow deposition increases annually by about 4%. Changes in albedo and surface dust content also impact the shortwave energy flux at the surface. With SNICAR integration, net shortwave flux into the surface changes by -1.26 W/m^2. Changes in albedo also show a similar distribution to dust deposition over the globe.

Real snow albedos are much lower than the dust-free albedos due to the high amount of dust deposition on Mars, and higher susceptibility of CO_2 snow albedo to dust darkening as compared to H_2O snow. Dust is one of the key elements in determining the climate state of Mars. We quantified several diagnostic radiative flux quantities for this study. First, we diagnosed the instantaneous difference between the SNICAR-MGCM net shortwave flux and what the flux would have been if there were instead bare ground where the model predicts dusty cryosphere. Over snow-covered regions, we calculated this cryosphere forcing term to be -2.25 W/m^2. Second, we quantified the instantaneous difference in net shortwave flux between the dust-laden cryosphere and the pure cryosphere; i.e., between the SNICAR-MGCM result and the result that would have been obtained if the predicted snow-covered areas had contained no dust. Over snow-covered regions, we calculated this difference to be 3.33 W/m^2, which is about 1.5 times greater than the impact of the dust-laden cryosphere relative to the no-cryosphere case.

We also achieve a better correlation between dust deposition (as gauged by atmospheric dust optical depth) and surface albedo with the SNICAR-MGCM, indicating higher dependency of surface albedo on dust. We expect this study will lead to better understanding of various other physical processes connected (directly or indirectly) with surface albedo on Mars, including energy transfer and dust movement.

Acknowledgements

Authors are grateful to Claire Newman (the associate editor), and two anonymous reviewers for their constructive and insightful suggestions, which lead to the significant improvement of the manuscript. The data used to generate maps/plots in the paper can be directly accessed from *https://deepblue.lib.umich.edu/data/concern/generic_works/x633f129g*. The web version of Mars Climate Database v5.2 created using original-MGCM can be interactively accessed on the web at: *http://www-mars.lmd.jussieu.fr/mars/access.html*. A single-layer implementation of SNICAR can be operated interactively on the web at: *http://snow.engin.umich.edu*.

References

Bony, S., R. Colman, R., V. M. Kattsov, R. P. Allan, C. S. Bretherton, J-L., Dufresne, A. Hall, S. Hallegatte, M. M. Holland, W. Ingram, D. A. Randall, B. J. Soden, G. Tselioudis, and M. J. Webb (2006), How Well Do We Understand and Evaluate Climate Change Feedback Processes?, J. Climate, 19, 3445–3482, doi: 10.1175/JCLI3819.1.

Brown, A. J., W. M. Calvin, P. C. McGuire, and S. L. Murchie (2010), Compact Reconnaissance Imaging Spectrometer for Mars (CRISM) south polar mapping: First Mars year of observations, J. Geophys. Res., 115, E00D13, doi:10.1029/2009JE003333.

Brown, A. J., W. M. Calvin, and S. L. Murchie (2012), Compact Reconnaissance Imaging Spectrometer for Mars (CRISM) north polar springtime recession mapping: First 3 Mars years of observations, J. Geophys. Res., 117, E00J20, doi:10.1029/2012JE004113.

Brown, A. J., W. M. Calvin, P. Becerra, and S. Byrne (2016), Martian north polar cap summer water cycle, Icarus, 277, 401-415, doi:10.1016/j.icarus.2016.05.007.

Cantor, B. A. (2007), MOC observations of the 2001 Mars planet-encircling dust storm, Icarus, 186(1), 60-96, doi:10.1016/j.icarus.2006.08.019.

Clancy, R. T., B. J. Sandor, M. J. Wolff, P. R. Christensen, M. D. Smith, J. C. Pearl, B. J. Conrath, and R. J. Wilson (2000), An intercomparison of ground-based millimeter, MGS TES, and Viking atmospheric temperature measurements: Seasonal and interannual variability of temperatures and dust loading in the global Mars atmosphere, J. Geophys. Res., 105(E4), 9553–9571, doi:10.1029/1999JE001089.

Flanner, M. G., C. S. Zender, J. T. Randerson, and P. J. Rasch (2007), Present day climate forcing and response from black carbon in snow, J. Geophys. Res., 112, D11202, doi:10.1029/2006JD008003.

Flanner, M. G., C. S. Zender, P. G. Hess, N. M. Mahowald, T. H. Painter, V. Ramanathan, and P. J. Rasch (2009), Springtime warming and reduced snow cover from carbonaceous particles, Atmos. Chem. Phys., 9, 2481-2497, doi:10.5194/acp-9-2481-2009.

Flato, G., J. Marotzke, B. Abiodun, P. Braconnot, S. C. Chou, W. Collins, P. Cox, F. Driouech, S. Emori, V. Eyring, C. Forest, P. Gleckler, E. Guilyardi, C. Jakob, V. Kattsov, C. Reason and M. Rummukainen (2013), Evaluation of Climate Models. In: Climate Change 2013: The Physical Science Basis. Contribution of Working Group I to the Fifth Assessment Report of the Intergovernmental Panel on Climate Change [T. F. Stocker, D. Qin, G.-K. Plattner, M. Tignor, S. K. Allen, J. Boschung, A. Nauels, Y. Xia, V. Bex and P. M. Midgley (eds.)]. Cambridge

University Press, Cambridge, United Kingdom and New York, NY, USA, 741–866, doi:10.1017/CBO9781107415324.020.

Forget, F., F. Hourdin, and O. Talagrand (1998), CO_2 snowfall on Mars: Simulation with a general circulation model. Icarus, 131(2), 302-316, doi:10.1006/icar.1997.5874.

Forget,F., F. Hourdin, R. Fournier, C. Hourdin, O. Talagrand, M. Collins, S. R. Lewis, and J.-P. Huot (1999), Improved general circulation models of the Martian atmosphere from the surface to above 80 km, J. Geophys. Res., 104, 24,155–24,176. doi: 10.1029/1999JE001025 .

Guzewich, S. D., A. D. Toigo, and H. Wang (2017), An investigation of dust storms observed with the Mars Color Imager, Icarus, 289, 199-213, doi: 10.1016/j.icarus.2017.02.020.

Haberle, R. M., C. B. Leovy, and J. B. Pollack (1982), Some effects of global dust storms on the atmospheric circulation of Mars, Icarus, 50(2-3), 322-367, doi: 10.1016/0019-1035(82)90129-4.

Hansen, J. E., and L. D. Travis (1974), Light scattering in planetary atmospheres, Space Science Reviews, 16(4), 527-610.

Hess, S. L., J. A. Ryan, J. E. Tillman, R. M. Henry, and C. B. Leovy (1980), The annual cycle of pressure on Mars measured by Viking Landers 1 and 2, Geophys. Res. Lett., 7: 197–200. doi:10.1029/GL007i003p00197.

Hourdin, F., P. Le Van, F. Forget, and O. Talagrand (1993), Meteorological variability and the annual surface pressure cycle on Mars, J. Atmos. Sci., 50(21), 3625-3640, doi: 10.1175/1520-0469(1993)050<3625:MVATAS>2.0.CO;2.

Hourdin, F., F. Forget, and O. Talagrand (1995), The sensitivity of the Martian surface pressure and atmospheric mass budget to various parameters: A comparison between numerical simulations and Viking observations, J. Geophys. Res., 100(E3), 5501–5523, doi:10.1029/94JE03079.

Jakosky, B. M., and C. B. Farmer (1982), The seasonal and global behavior of water vapor in the Mars atmosphere: Complete global results of the Viking Atmospheric Water Detector Experiment, J. Geophys. Res., 87(B4), 2999–3019, doi:10.1029/JB087iB04p02999.

Kieffer, H. H., and T. N. Titus (2001), TES mapping of Mars' north seasonal cap, Icarus, 154(1), 162-180, doi:10.1006/icar.2001.6670.

Kieffer, H. H., T. N. Titus, K. F. Mullins, and P. R. Christensen (2000), Mars south polar spring and summer behavior observed by TES: Seasonal cap evolution controlled by frost grain size, J. Geophys. Res., 105(E4), 9653–9699, doi:10.1029/1999JE001136.

Kieffer, H. H. (1990), H_2O grain size and the amount of dust in Mars' Residual north polar cap, J. Geophys. Res., 95(B2), 1481–1493, doi:10.1029/JB095iB02p01481.

Labs, D., H. Neckel (1968), The Radiation of the Solar Photosphere from 2000 Å to 100 µm. Zeitschrift fur Astrophysik, 69, 1.

Madeleine, J.-B., F. Forget, E. Millour, L. Montabone, and M. J. Wolff (2011), Revisiting the radiative impact of dust on Mars using the LMD Global Climate Model, J. Geophys. Res., 116, E11010, doi:10.1029/2011JE003855.

Maltagliati, L., D. V. Titov, T. Encrenaz, R. Melchiorri, F. Forget, H. U. Keller and J. P. Bibring (2011), Annual survey of water vapor behavior from the OMEGA mapping spectrometer onboard Mars Express, Icarus, 213(2), 480-495, doi: 10.1016/j.icarus.2011.03.030

Montabone, L., F. Forget, E. Millour, R. J. Wilson, S. R. Lewis, B. Cantor, D. Kass, A. Kleinböhl, M. T. Lemmon, M. D. Smith and M. J. Wolff (2015), Eight-year climatology of dust optical depth on Mars, Icarus, 251, 65-95, doi: 10.1016/j.icarus.2014.12.034.

Newman, C. E., S. R. Lewis, P. L. Read, and F. Forget, (2002a), Modeling the Martian dust cycle, 1, Representations of dust transport processes, J. Geophys. Res., 107(E12), 5123, doi:10.1029/2002JE001910.

Newman, C. E., S. R. Lewis, P. L. Read, and F. Forget, (2002b), Modeling the Martian dust cycle, 2, Multiannual radiatively active dust transport simulations, J. Geophys. Res., 107(E12), 5124, doi:10.1029/2002JE001920.

Navarro, T.,J.-B. Madeleine, F. Forget, A. Spiga, E. Millour, F. Montmessin, and A. Määttänen (2014), Global climate modeling of the martian water cycle with improved microphysics and radiatively active water ice clouds, J. Geophys. Res. 119 (7), 1479–1495. doi: 10.10 02/2013JE0 04550 .

Pottier, A., F. Forget, F. Montmessin, T. Navarro, A. Spiga, E. Millour, A. Szantai, J.-B. Madeleine (2017), Unraveling the martian water cycle with high-resolution global climate simulations, Icarus, 291, 82-106, doi: 10.1016/j.icarus.2017.02.016.

Randall, D.A., R. A. Wood, S. Bony, R. Colman, T. Fichefet, J. Fyfe, V. Kattsov, A. Pitman, J. Shukla, J. Srinivasan, R. J. Stouffer, A. Sumi and K. E. Taylor (2007), Climate Models and Their Evaluation. In: Climate Change 2007: The Physical Science Basis. Contribution of Working Group I to the Fourth Assessment Report of the Intergovernmental Panel on Climate Change [Solomon, S., D. Qin, M. Manning, Z. Chen, M. Marquis, K. B. Averyt, M. Tignor and H. L. Miller, (eds.)]. Cambridge University Press, Cambridge, United Kingdom and New York, NY, USA.

Shell, K. M., J. T. Kiehl, and C.A. Shields (2008), Using the radiative kernel technique to calculate climate feedbacks in NCAR's community atmospheric model, J. Clim. 21, 2269-2282, doi:10.1175/2007JCLI2044.1.

Singh, D., and Flanner, M. G. (2016), An improved carbon dioxide snow spectral albedo model: Application to Martian conditions, J. Geophys. Res. Planets, 121, 2037–2054, doi:10.1002/2016JE005040.

Singh, D., Flanner, M. G., and Perket, J. (2015), The global land shortwave cryosphere radiative effect during the MODIS era, The Cryosphere, 9, 2057-2070, doi:10.5194/tc-9-2057-2015.

Smith, M. D. (2002), The annual cycle of water vapor on Mars as observed by the Thermal Emission Spectrometer, J. Geophys. Res., 107(E11), 5115, doi:10.1029/2001JE001522.

Soden, B. J., I. M. Held, R. Colman, K. M. Shell, J. T. Kiehl, and C. A. Shields (2008), Quantifying climate feedbacks using radiative kernels, J. Clim., 21(14), 3504–3520, doi:10.1175/2007JCLI2110.1.

Wang, H., and M. I. Richardson (2015), The origin, evolution, and trajectory of large dust storms on Mars during Mars years 24–30 (1999–2011), Icarus, 251, 112-127, doi: 10.1016/j.icarus.2013.10.033.

Warren, S. G. (1984), Impurities in snow: Effects on albedo and snowmelt, Annals of Glaciology, 5(1), 177-179, doi:10.3198/1984AoG5-1-177-179.

Winton, M. (2006), Surface albedo feedback estimates for the AR4 climate models, J. Clim. 19, 359-365, doi:10.1175/JCLI3624.1.

Wiscombe, W. J., and S. G. Warren (1980), A Model for the Spectral Albedo of Snow. II: Snow containing atmospheric aerosols, J. Atmos. Sci., 37(12), 2734-2745, doi:10.1175/1520-0469(1980)037<2734:AMFTSA>2.0.CO;2.

Wolff, M. J., R. T. Clancy, J. D. Goguen, and M. C. Malin, and B. A. Cantor (2010), Ultraviolet dust aerosol properties as observed by MARCI, Icarus, 208(1), 143-155, doi:10.1016/j.icarus.2010.01.010.

Wolff, M. J., M. D. Smith, R. T. Clancy, R. Arvidson, M. Kahre, F. Seelos IV, S. Murchie, and H. Savijarvi (2009), Wavelength dependence of dust aerosol single scattering albedo as observed by the Compact Reconnaissance Imaging Spectrometer, J. Geophys. Res., 114, E00D04, doi:10.1029/2009JE003350.

Wolff, M.J., M. D. Smith, R. T. Clancy, N. Spanovich, B. A. Whitney, M. T. Lemmon, J. L. Bandfield, D. Banfield, A. Ghosh, G. Landis, P. R. Christensen, J. F. Bell III and S. W. Squyres

(2006), Constraints on dust aerosols from the Mars Exploration Rovers using MGS overflights and Mini TES, J. Geophys. Res., 111, E12S17, doi:10.1029/2006JE002786.

Wood, S. E., and D. A. Paige (1992), Modeling the Martian seasonal CO_2 cycle 1. Fitting the Viking Lander pressure curves, Icarus, 99(1), 1-14, doi:10.1016/0019-1035(92)90166-5.

Zurek, R. W., and L. J. Martin (1993), Interannual variability of planet-encircling dust storms on Mars, J. Geophys. Res., 98(E2), 3247–3259, doi:10.1029/92JE02936.

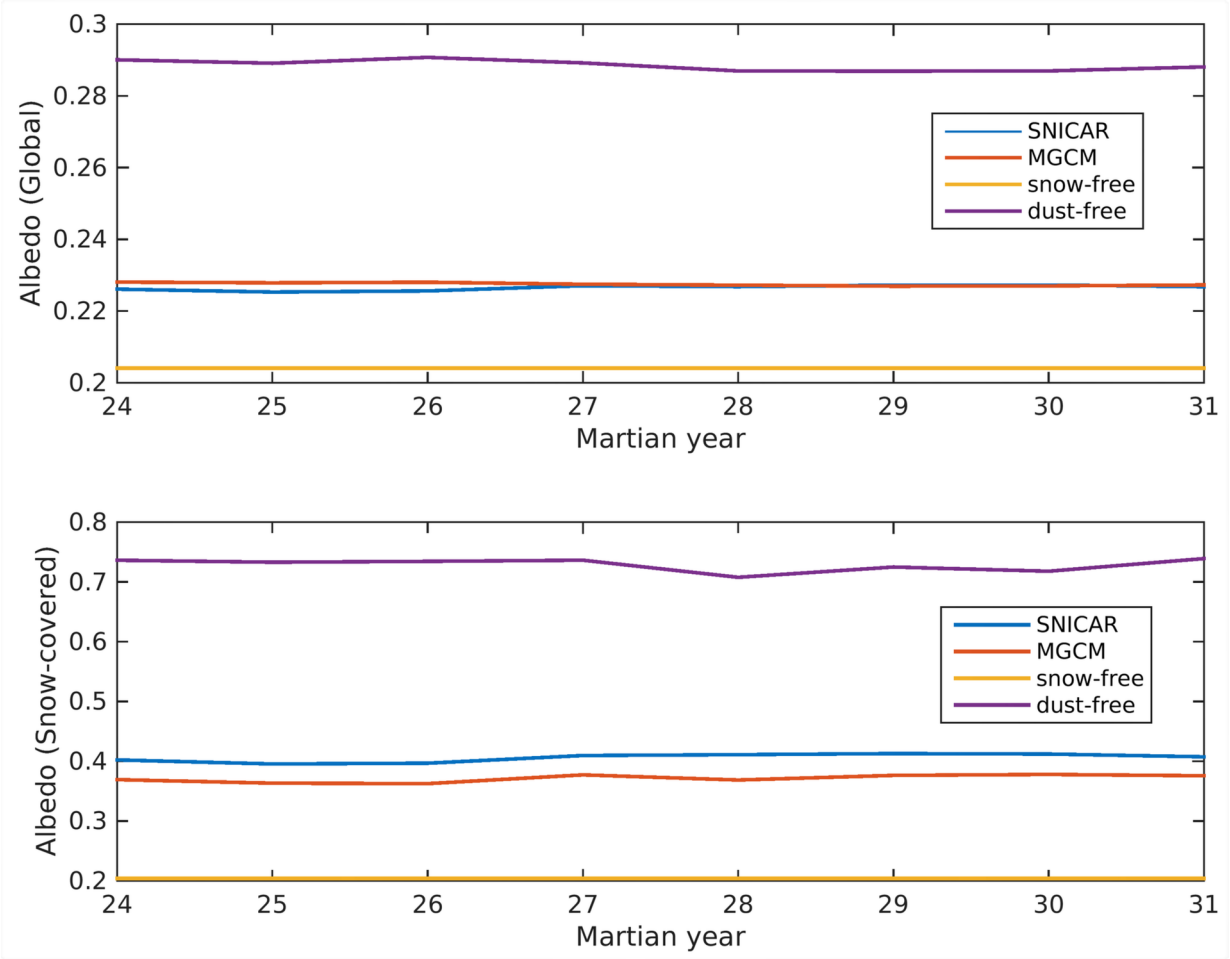

2017JE005368-f01-z-.tif

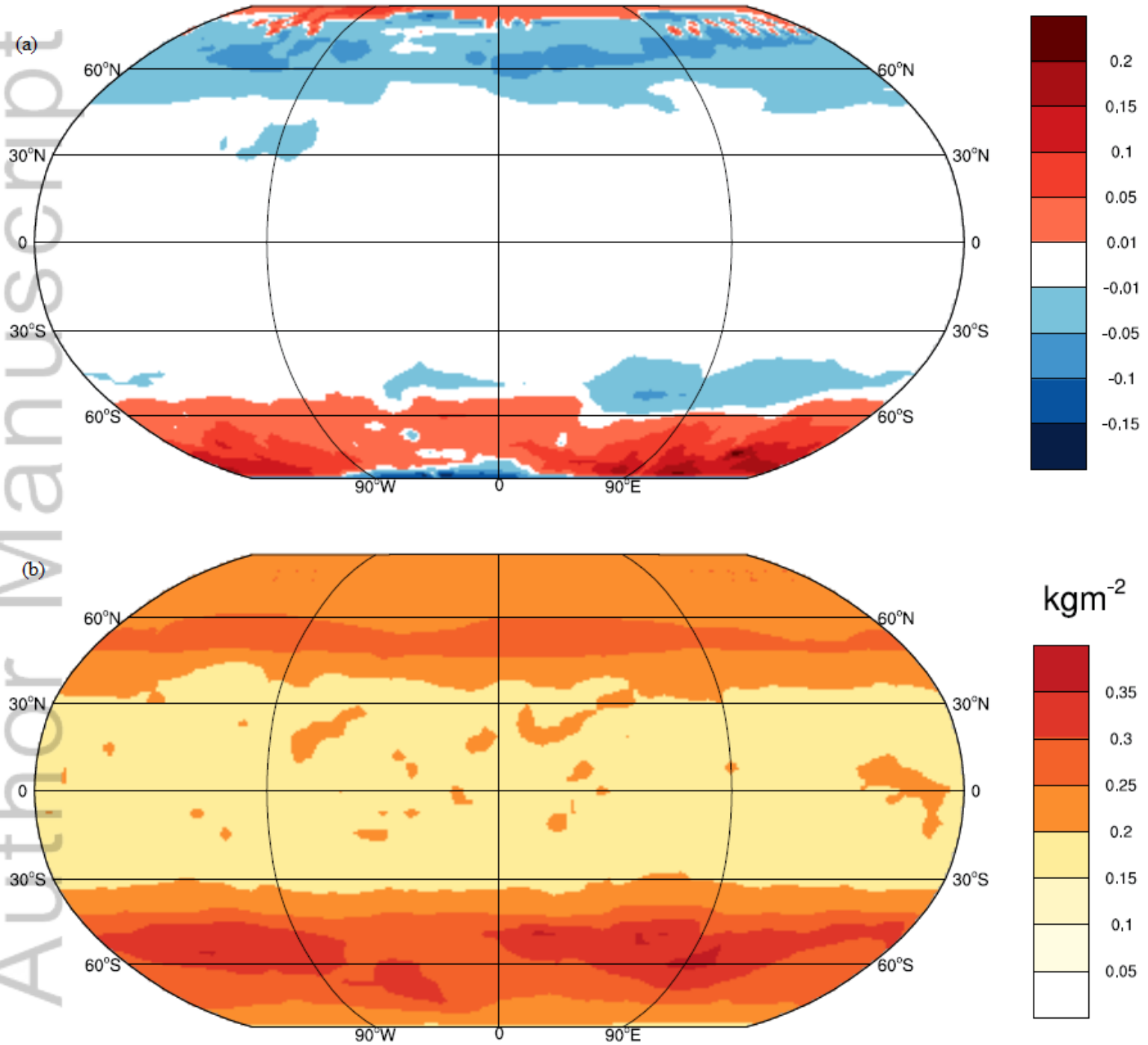

2017JE005368-f02-z-.tif

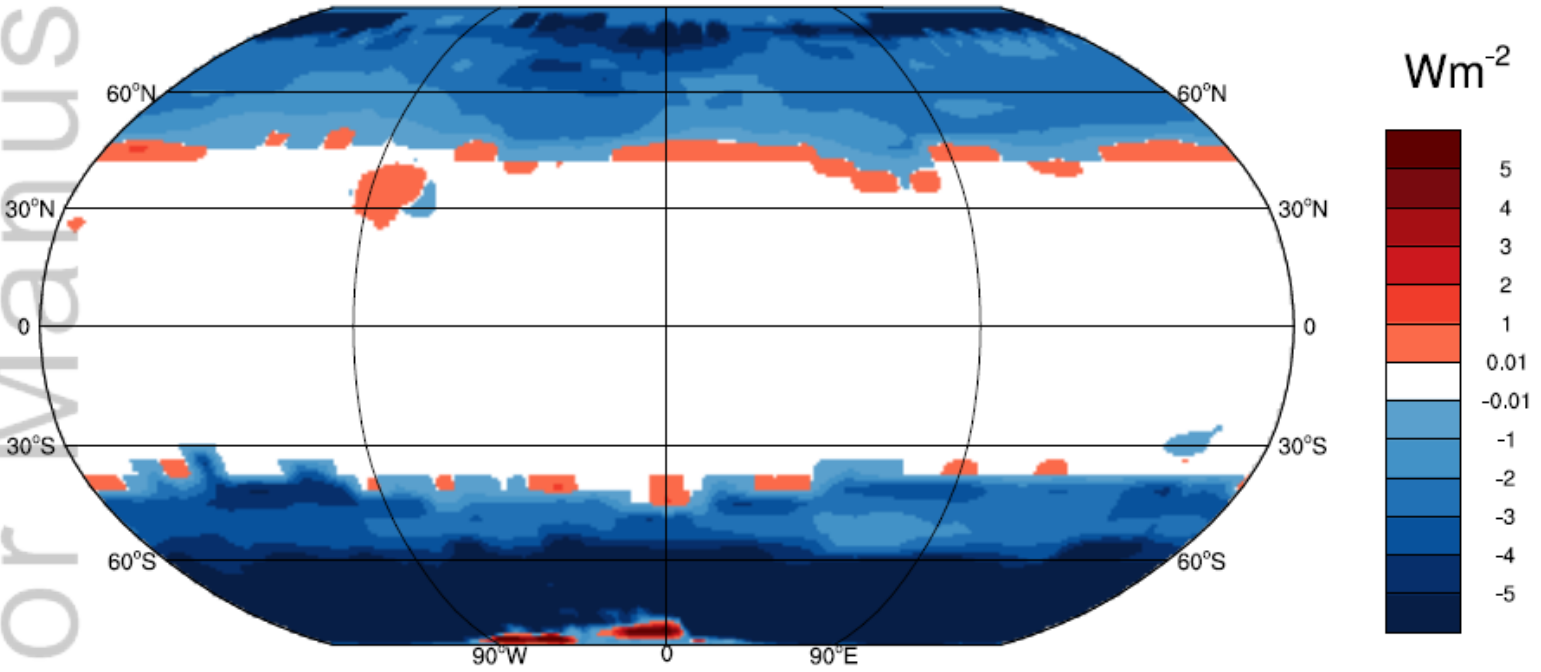

2017JE005368-f03-z-.tif

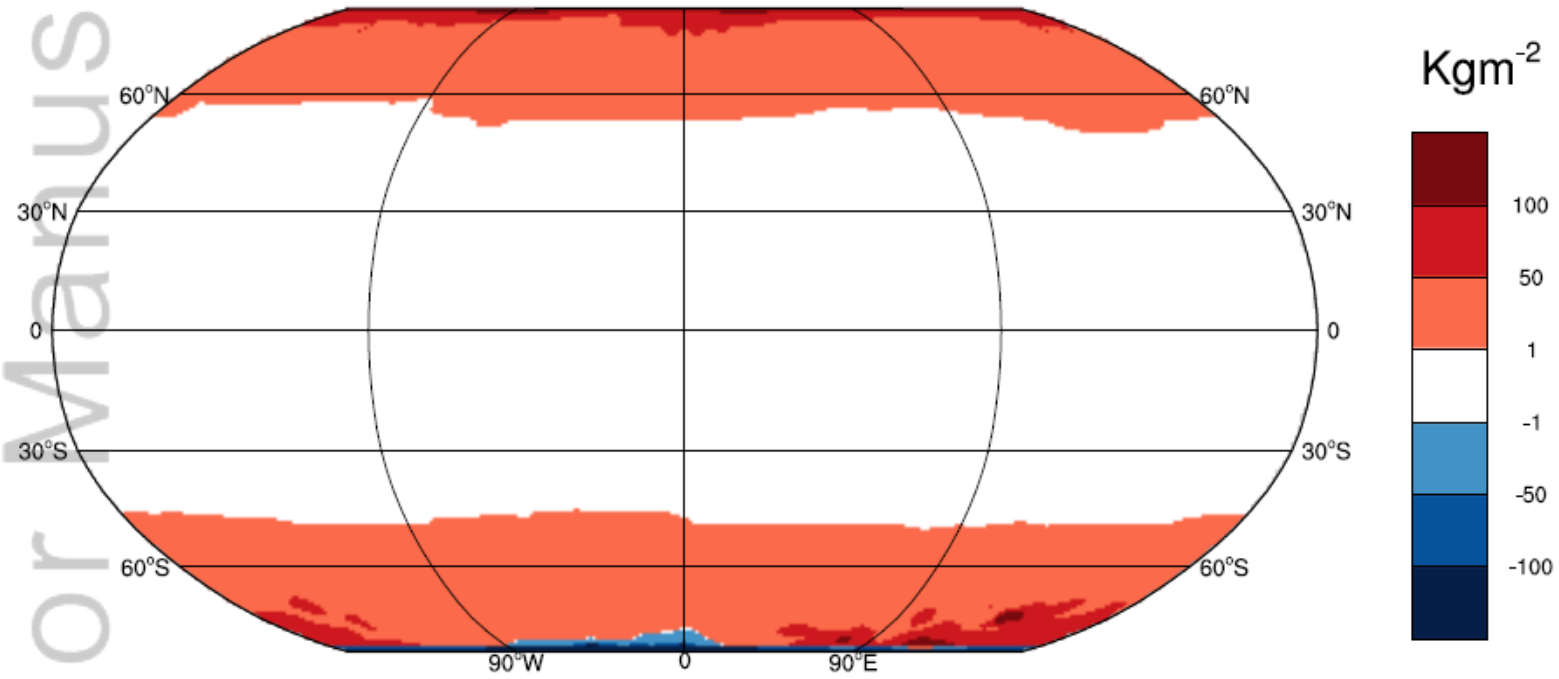

2017JE005368-f04-z-.tif

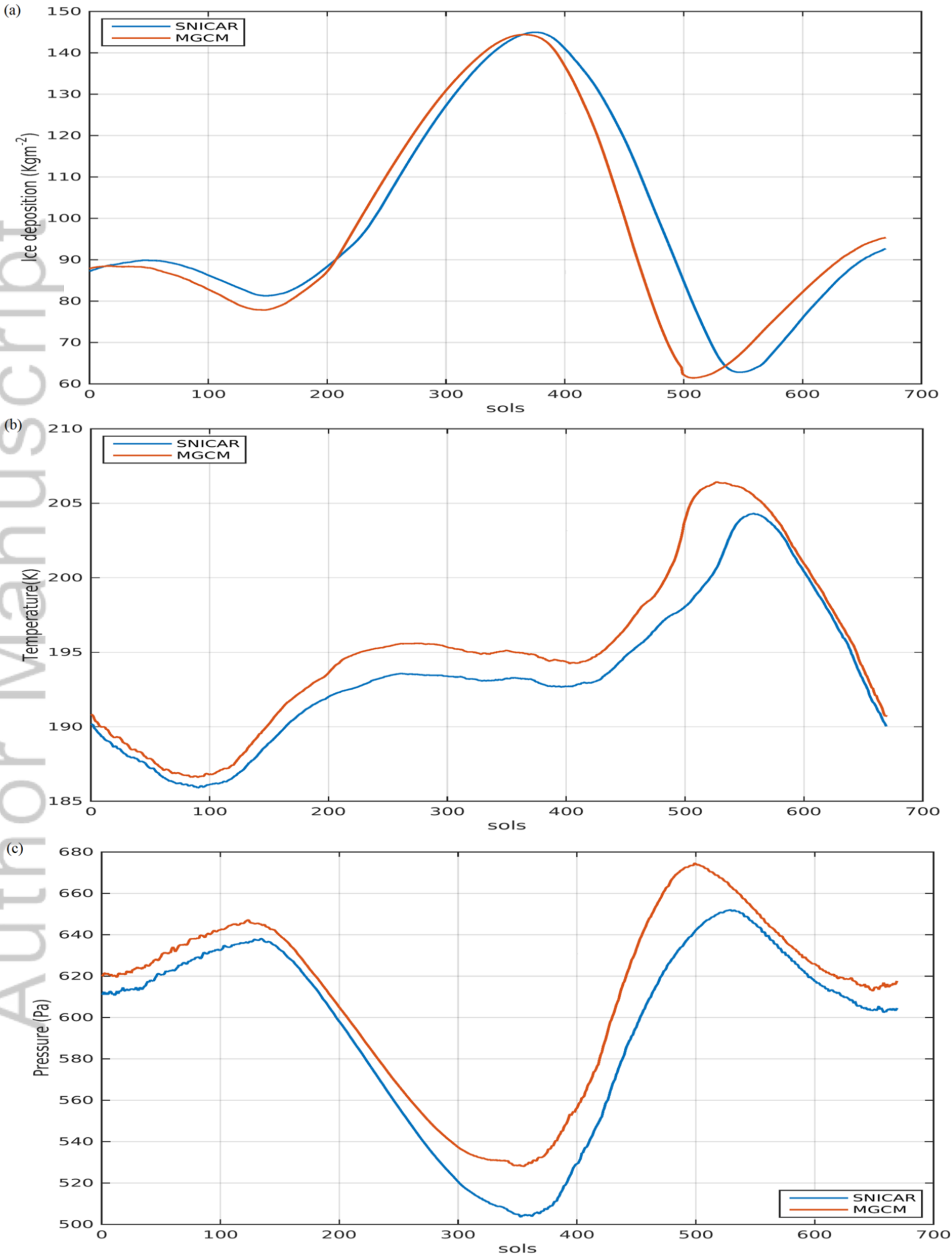

2017JE005368-f05-z-tif

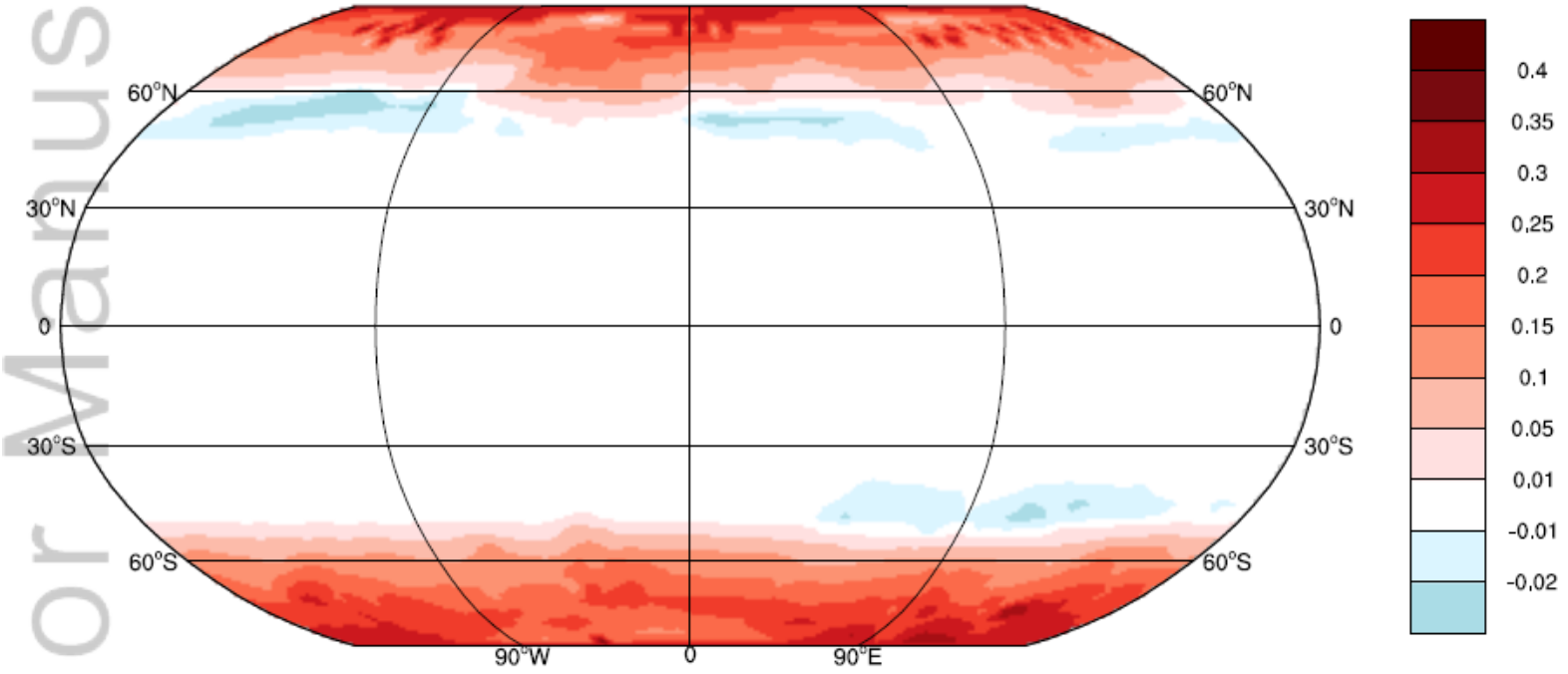

2017JE005368-f06-z-.tif

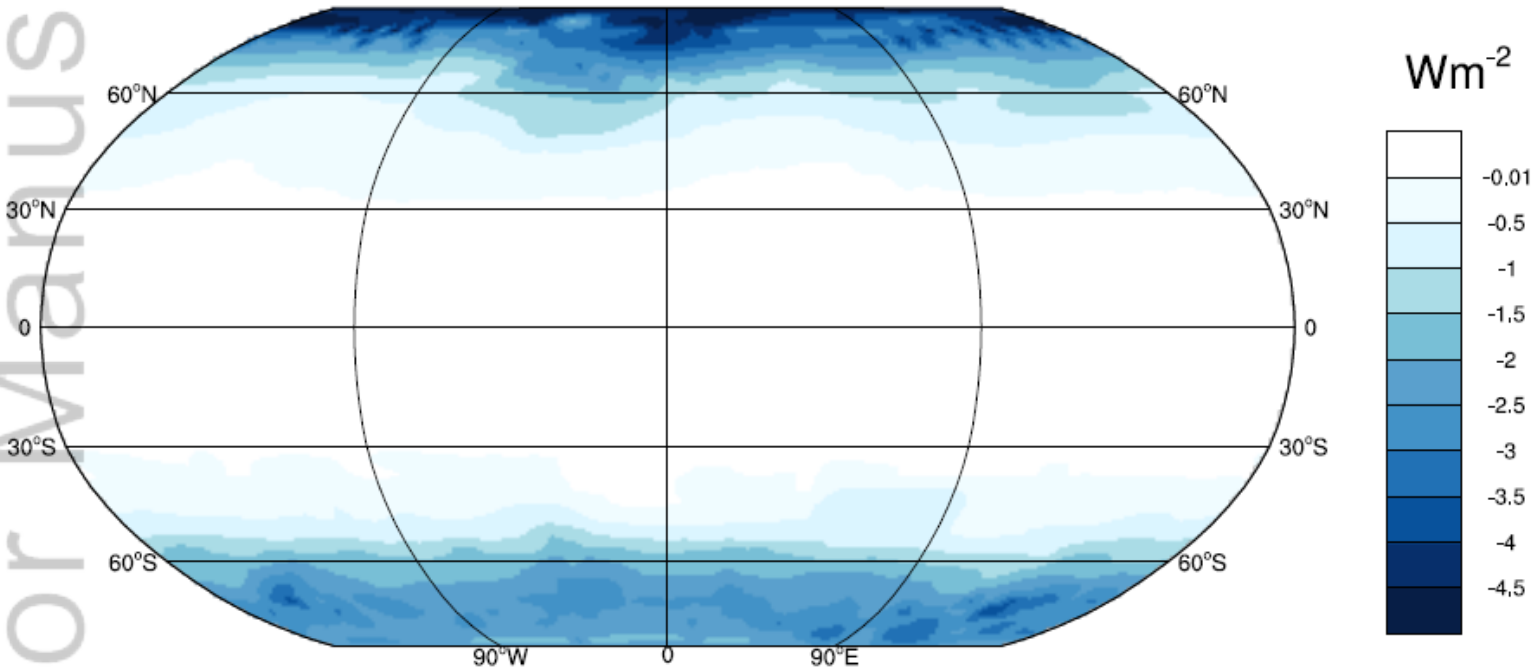

2017JE005368-f07-z-.tif

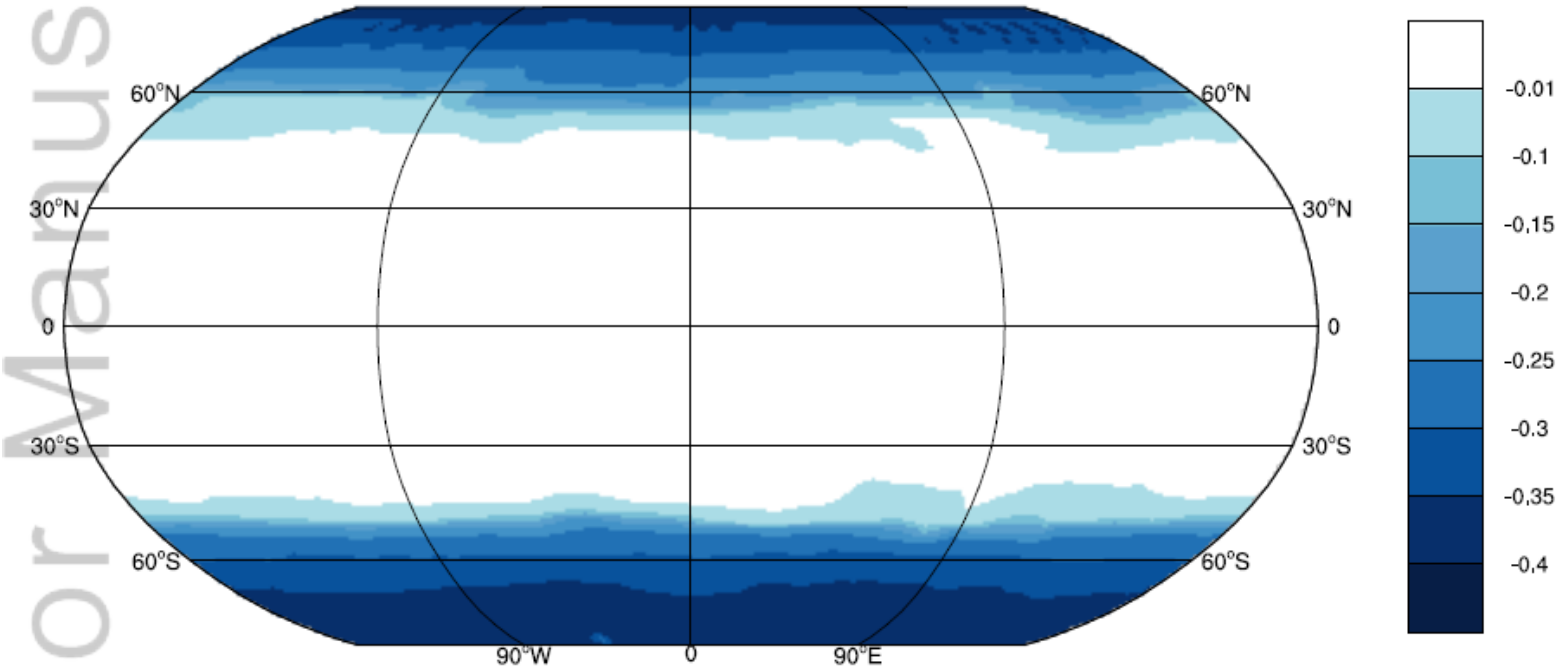

2017JE005368-f08-z-.tif

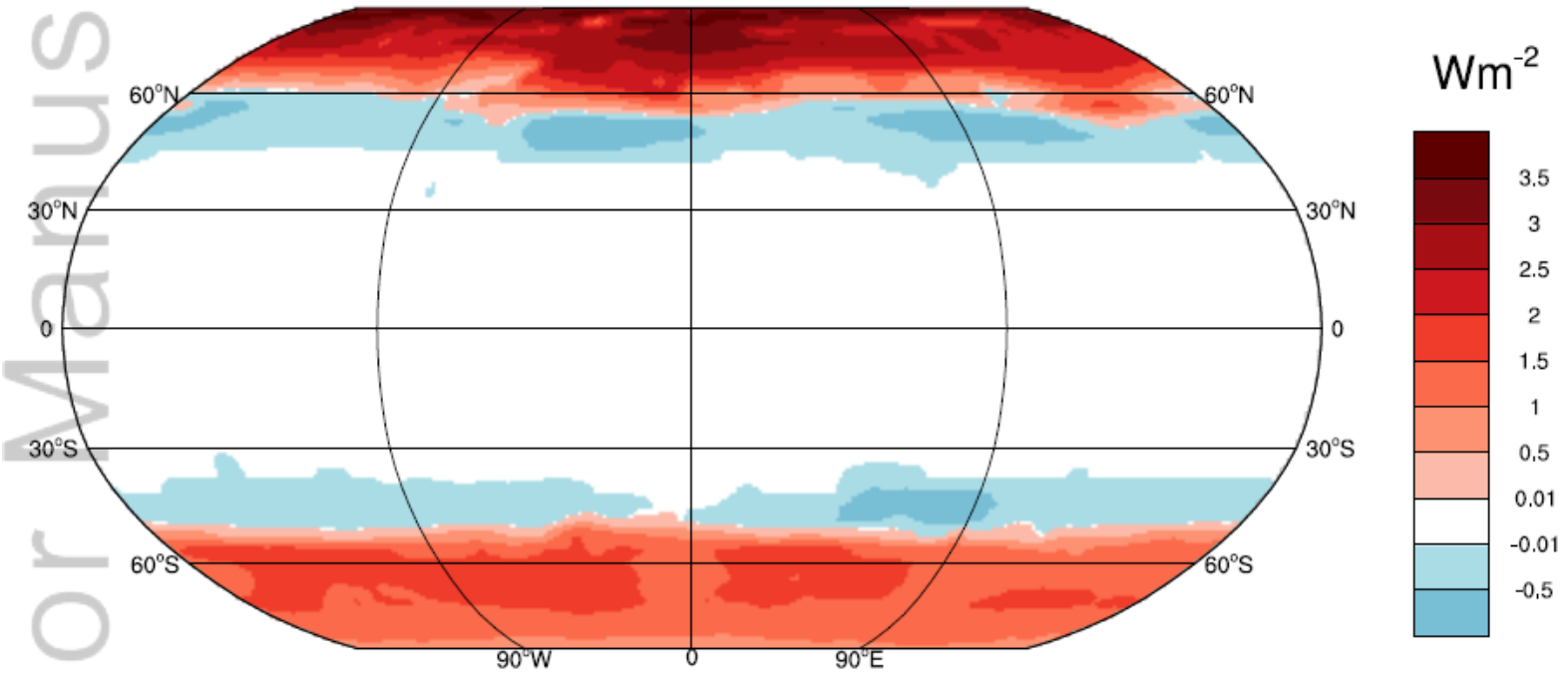

2017JE005368-f09-z-.tif

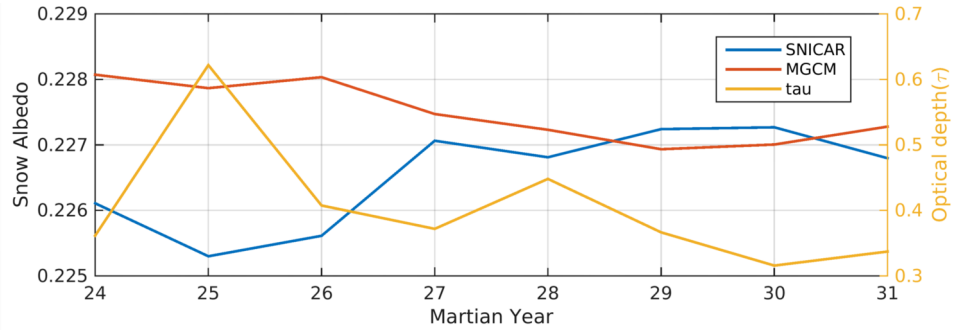

2017JE005368-f10-z-.tif

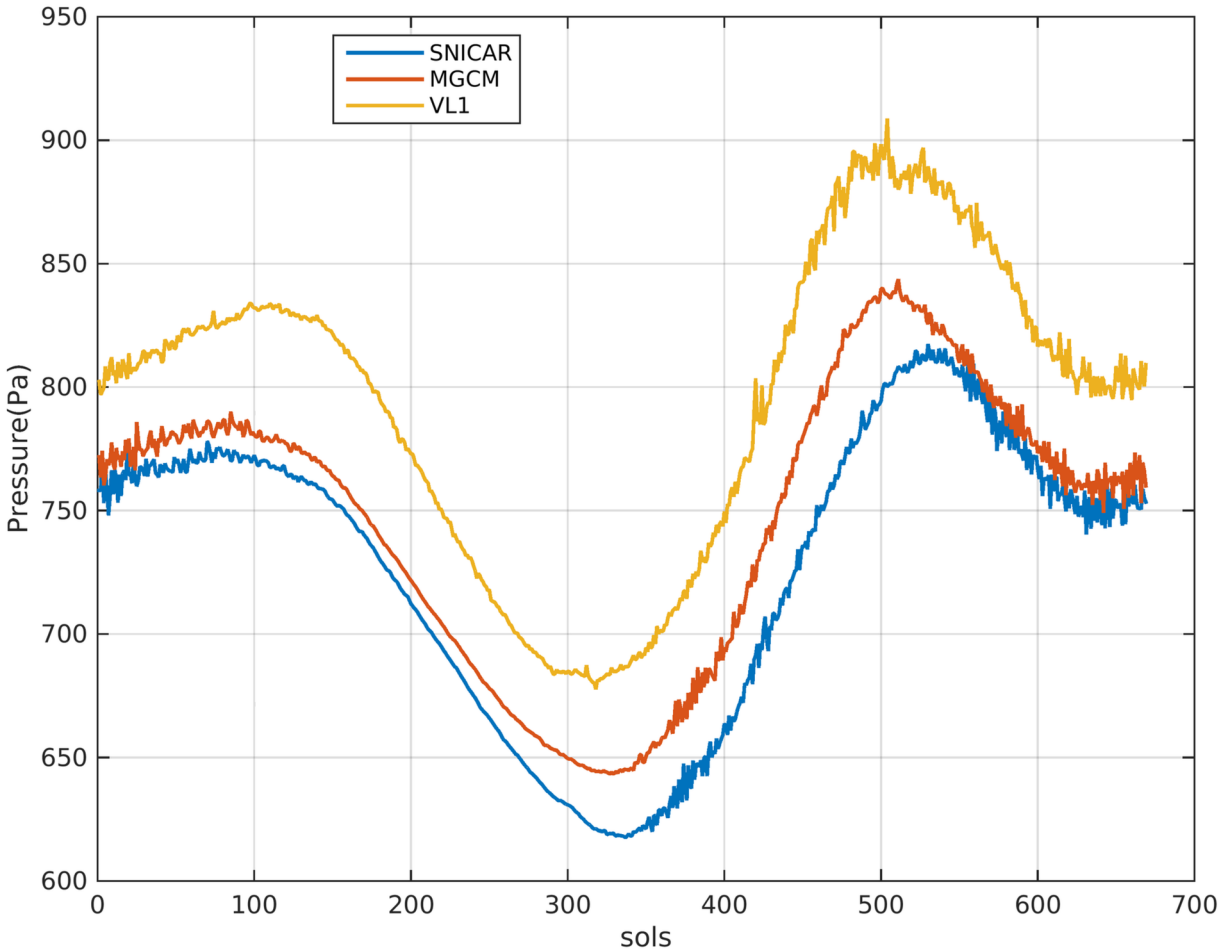

2017JE005368-f11-z-.tif